

Two end variable singularity boundary elements and their applications in crack–crack interaction problems

N. K. Mukhopadhyay^{1,*}, S. K. Maiti^{2,†} and A. Kakodkar¹

¹Reactor Design and Development Group, Bhabha Atomic Research Centre, Mumbai 400085, India

²Mechanical Engineering Department, Indian Institute of Technology, Bombay, Mumbai 400076, India

SUMMARY

Two new boundary elements have been proposed for simulation of variable order singularities at the two ends of an element in two dimensions. The first can model the variable order strain singularity at both the ends of the element. The second element can do both the strain and traction singularities simultaneously. The elements are useful for studying the interaction of singularities as in the case of multiple neighbouring cracks in a domain. They are employed here for the computation of stress intensity factors (SIFs) in the crack–crack interaction problems. To improve the accuracy of such computations further a modified crack closure integral (MCCI) based method for mechanical and/or thermal loading is presented. Examples of mode I crack and mixed mode problems under mechanical loading are studied to illustrate the performance of the proposed elements and the MCCI-based calculations. The effects of the order of Gauss quadrature associated with such elements on the accuracy of the SIFs are also reported. Copyright © 2000 John Wiley & Sons, Ltd.

KEY WORDS: two end variable order strain singularity element; two end variable order traction singularity element; boundary element; modified crack closure integral; stress intensity factor; accuracy of SIF computation

INTRODUCTION

In an elastic media, singularity in the first derivative of field variable occurs due to the presence of a crack. In practical applications there are many situations where a structure contains more than one crack. This implies that there are as many singularity points in the structure as the number of crack tips. When the cracks are situated in close proximity the neighbouring singularities will interact. A macrocrack surrounded by small cracks or ‘microcracks’ is a typical example. Many investigators e.g. Chudnovsky and Kachanov [1], Kachanov [2], Raju [3], Hori and Nemat-Nasser [4], Rubeinstein and Choi [5], Lam and Phua [6], etc., have shown that interaction with a microcrack array can significantly alter the stress intensity factor (SIF) at the main crack tip.

* Correspondence to: N. K. Mukhopadhyay, Reactor Design and Development Group, Bhabha Atomic Research Centre, Mumbai 400085, India

† E-mail: nirmalk@apsara.barc.ernet.in

‡ E-mail: skmaiti@me.iitb.ernet.in

In general, the order of singularity at the tip of a crack in an elastic media is the square root singularity. In the case of a kinked crack, there are neighbouring singularities at the knee and the crack tip. The order of singularity at the crack tip is the square root singularity, but the order at the knee varies with the knee angle [7]. If there are a number of small cracks surrounding the kinked crack this gives rise to the problem of neighbouring singularities. A zigzag crack due to stress corrosion cracking is another example which can also lead to a problem of neighbouring singularities. In the case of heat conduction too, the problem of neighbouring singularities can occur, for example, if there is an interruption of heat flow through an isotropic media by a number of cracks lying in close proximity. To address the related boundary element modelling two things are important, modelling of variable order singularity and neighbouring singularities.

Many investigators [8–10] have proposed special finite elements to model variable order singularity because modelling of singularity has a significant influence on the accuracy of results. To model neighbouring singularities a large number of such elements are required. Dutta *et al.* [11] and Maiti [12] proposed multicorner variable order singularity finite elements to handle such problems in a challenging manner. These elements [12] can handle up to three neighbouring singularities. No attempt has so far been made to develop similar elements in the boundary element method (BEM).

For a singularity finite element based on the displacement formulation, the assumed displacement field is required to ensure only the strain singularity. The stress singularity is automatically guaranteed as stresses are calculated directly from the strains. In the case of heat conduction analysis using such elements, the heat flux singularity is automatically ensured since the heat flux is directly related to the temperature derivative. Thus there is no special effort required to ensure singularity in the stress and heat flux, respectively. In contrast, in the BEM, the displacement (or temperature) and traction (or heat flux) are treated as separate entities. The incorporation of singularity in, for example, the displacement does not automatically guarantee the required singularity in the case of traction. Special efforts are required to ensure the total modelling of singularities, i.e. simultaneous modelling of both strain and traction singularities.

The modelling of the singularities has received considerable attention in the BEM [13–22]. In 1981, Blandford *et al.* [13], introduced a special element, known as ‘traction singularity element’ for modelling of both the singularities. In the BEM, the most common square-root singularity has been at the centre of focus and the problem of variable order singularity or neighbouring variable order singularity problems has not received much attention. Only recently the present authors [23] have proposed two variable order singularity boundary elements and its usefulness in computing the stress intensity factors (SIFs) in two dimensions have been shown. The first element, termed as ‘variable strain singularity’ (VSS) element, ensures the variable order strain singularity at the crack tip. The second element, called ‘variable strain and traction singularity’ (VSTS) element, helps to model both the variable order strain and traction singularities simultaneously. The MCCI-based calculations are also presented to evaluate the SIFs from crack tip displacements and tractions. These elements can be employed to solve the problem of variable order singularities. The problem of modelling of neighbouring variable order singularities remain open to investigations. This has provided the main motivation for the present study. Developments of two such elements and their applications in crack–crack interaction problems are presented.

Though the SIFs can be evaluated through the most common displacement method, the MCCI technique offers better accuracy [24–27]. The use of MCCI in conjunction with the special elements are examined. When these special crack tip elements are employed for any analysis the

analyst is required to handle a product of two singularity terms for the evaluation of coefficients of the simultaneous equations. The integration of the singular kernels is performed through the standard Gauss quadrature, e.g. Reference [28, 29]. As a result the order of Gauss quadrature [30] plays a crucial role in the accuracy of the results. How does the order of Gauss quadrature affect the accuracy of the SIFs is also examined in this paper.

ELEMENT FORMULATION

Two end strain singularity (TESS) element

A variable order singularity in the displacement derivative is obtained by manipulating the element displacement shape functions of a quadratic or 3-noded element. This calls for an adjustment so as to give rise to an infinite slope in the field variable at the point of interest. A set of such shape functions [23] are

$$\begin{aligned} N_1 &= 2^c [- (r/l)^c + (r/l)^{c+1}] + 1 - (r/l) \\ N_2 &= 2^{c+1} [(r/l)^c - (r/l)^{c+1}] \\ N_3 &= 2^c [- (r/l)^c + (r/l)^{c+1}] - (r/l) + 1 \end{aligned} \quad (1)$$

where r is the distance from the crack tip, l is the length of the crack tip element and c is the singularity parameter. This element is called VSS element. The shape functions fulfil the rigid-body and the constant-strain criteria. The displacement and traction are represented by

$$u = N_1 u_1 + N_2 u_2 + N_3 u_3 \quad (2)$$

$$t = N_1 t_1 + N_2 t_2 + N_3 t_3 \quad (3)$$

When these elements are employed, the field variable (say, displacement) varies as r^c , $0 < c < 1$, and the derivative of field variable (strain) varies as r^{c-1} the order of singularity is $1 - c$. $c = 0.5$ gives the common square-root strain singularity.

Shape functions to suit the singularity at the two ends can be written separately. To get a single set of shape functions to represent singularities simultaneously at the two ends simple superposition can be employed

$$N_1 = w_1 \{ 2^c [- (r/l)^c + (r/l)^{c+1}] + 1 - (r/l) \} + w_2 \{ 2^d [- (1 - r/l)^d + (1 - r/l)^{d+1}] + 1 - (r/l) \} \quad (4)$$

Here the order of singularities at the end nodes are $(c - 1)$ and $(d - 1)$. r is the distance measured from the end node whose singularity parameter is c . For an equal bias $w_1 = w_2 = 0.5$ can be taken. Finally the two end strain singularity element shape functions are as follows (Figure 1(a))

$$\begin{aligned} N_1 &= 2^{c-1} [- (r/l)^c + (r/l)^{c+1}] + 2^{d-1} [- (1 - r/l)^d + (1 - r/l)^{d+1}] + 1 - (r/l) \\ N_2 &= 2^c [(r/l)^c - (r/l)^{c+1}] + 2^d [(1 - r/l)^d - (1 - r/l)^{d+1}] \\ N_3 &= 2^{c-1} [- (r/l)^c + (r/l)^{c+1}] + 2^{d-1} [- (1 - r/l)^d + (1 - r/l)^{d+1}] + (r/l) \end{aligned} \quad (5)$$

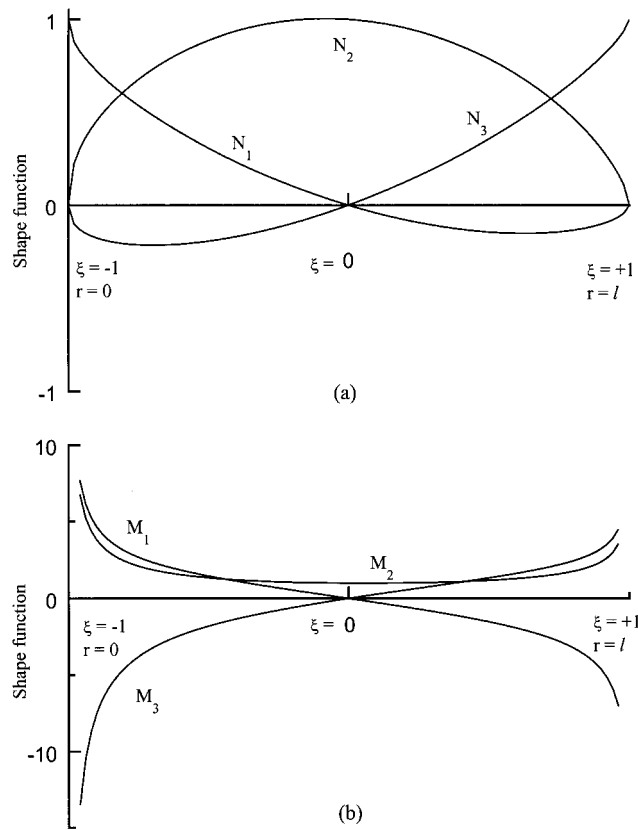


Figure 1. (a) Displacement and traction shape functions for TESS element and displacement shape functions for TESTS element. (b) Traction shape functions for TESTS element.

At the i th node N_i is unity and all other shape functions are zero. The derivatives of the shape functions are

$$\begin{aligned}
 \frac{\partial N_1}{\partial r} &= -\left(\frac{1}{l}\right) + 2^{c-1} \left(\frac{1}{l}\right) \left[-c \left(\frac{r}{l}\right)^{c-1} + (c+1) \left(\frac{r}{l}\right)^c \right] \\
 &\quad + 2^{d-1} \left(\frac{1}{l}\right) \left[d \left(\frac{l-r}{l}\right)^{d-1} - (d+1) \left(\frac{l-r}{l}\right)^d \right] \\
 \frac{\partial N_2}{\partial r} &= 2^c \left(\frac{1}{l}\right) \left[c \left(\frac{r}{l}\right)^{c-1} - (c+1) \left(\frac{r}{l}\right)^c \right] \\
 &\quad + 2^d \left(\frac{1}{l}\right) \left[-d \left(\frac{l-r}{l}\right)^{d-1} + (d+1) \left(\frac{l-r}{l}\right)^d \right]
 \end{aligned}
 \tag{6}$$

$$\begin{aligned} \frac{\partial N_3}{\partial r} = & \left(\frac{1}{l}\right) + 2^{c-1} \left(\frac{1}{l}\right) \left[-c \left(\frac{r}{l}\right)^{c-1} + (c+1) \left(\frac{r}{l}\right)^c \right] \\ & + 2^{d-1} \left(\frac{1}{l}\right) \left[d \left(\frac{l-r}{l}\right)^{d-1} - (d+1) \left(\frac{l-r}{l}\right)^d \right] \end{aligned}$$

It may be noted that all the derivatives display r^{c-1} singularity as $r \rightarrow 0$ and r^{d-1} as $r \rightarrow l$. The displacement field can now be written by adapting these shape functions and it gives rise to a strain singularity of order $(c-1)$ and one end (node 1) and $(d-1)$ at the other end (node 3). If the traction is expressed using these shape functions (Equation (5)), the traction does not display any singularity. Such an element is an example of the TESS element. In the heat conduction analysis, the TESS element ensures a variable order singularity at both the ends only in the radial temperature derivative ($\partial\phi/\partial r$).

It can be easily verified that $\sum N_i = 1$. This satisfies the rigid-body criteria. The proposed element also fulfils the constant strain criteria. This is checked in the following. Consider a situation where the temperature of the element is uniformly raised by T keeping the node 3 fully restrained. This gives rise to displacements $u_1 = \alpha T$ and $u_2 = \alpha T/2$, where α is the coefficient of thermal expansion. The element strain, on substitution

$$\frac{\partial u}{\partial x} = u_1 \frac{\partial N_1}{\partial x} + u_2 \frac{\partial N_2}{\partial x} = -\alpha T \quad (7)$$

The element therefore passes the constant strain requirement.

Two end strain and traction singularity (TESTS) element

To model both the strain and traction singularities, separate shape functions are needed to model the variable traction singularity. The required shape functions to cater for the traction singularity can be similar to the derivatives of the shape functions (Equation (5)) associated with the TESS element. A set of such shape functions is given below:

$$\begin{aligned} M_1 &= 2^{c-1} [(r/l)^{c-1} - (r/l)^c] + 2^d [(1-r/l)^{d-1} + (1-r/l)^d] + 1 - (r/l) \\ M_2 &= 2^{c-1} [(r/l)^{c-1} - (r/l)^c] + 2^{d-1} [(1-r/l)^{d-1} - (1-r/l)^d] \\ M_3 &= 2^c [- (r/l)^{c-1} + (r/l)^c] + 2^{d-1} [(1-r/l)^{d-1} - (1-r/l)^d] + (r/l) \end{aligned} \quad (8)$$

These shape functions are taken to have the following nodal values:

$$\begin{aligned} r/l = 0: M_1 &= \lim_{r \rightarrow 0} (r/l)^{c-1}, \quad M_2 = \lim_{r \rightarrow 0} (r/l)^{c-1}, \quad M_3 = \lim_{r \rightarrow 0} - (r/l)^{c-1} \\ r/l = \frac{1}{2}: M_1 &= 0, \quad M_2 = 1, \quad M_3 = 0 \\ r/l = 1: M_1 &= \lim_{r \rightarrow l} - \left(\frac{l-r}{l}\right)^{d-1}, \quad M_2 = \lim_{r \rightarrow l} \left(\frac{l-r}{l}\right)^{d-1}, \quad M_3 = \lim_{r \rightarrow l} \left(\frac{l-r}{l}\right)^{d-1} \end{aligned} \quad (9)$$

All the shape functions ensure an order of singularity $(c - 1)$ at node 1 as $(r \rightarrow 0)$ and $(d - 1)$ at node 3 as $(r \rightarrow l)$. The shape functions also satisfy $\sum M_i = 1$. The required variation of traction over the element can therefore be presented by

$$t = t_1 M_1 + t_2 M_2 + t_3 M_3 \tag{10}$$

A simultaneous representation of displacement field by shape functions (5) and the traction by shape functions (8) gives a TESTS element. This element guarantees singularities in both radial temperature derivative $(\partial\phi/\partial r)$ and heat flux $(\partial\phi/\partial n)$ when employed in the heat conduction analysis.

Adoption of the two new elements in an existing standard boundary element programme is a straightforward matter. However, proper care must be taken in evaluating the terms of $[H]$ and $[G]$ matrices, where $[H] \{u\} = [G] \{t\}$. Particularly, when both the load and field points are in the special singularity element, the origins $(r = 0)$ are different for the displacement and traction fields.

The two end singularity elements are compatible with the other two end singularity elements or variable singularity elements. These elements are to be surrounded by similar elements and not with ordinary quadratic elements. A few cases for possible applications are shown in Figure 2. In the case of two collinear neighbouring cracks (Figure 2(a)) both span AB and CD can be represented by the new elements. These elements are identified by 2. One end singularity elements

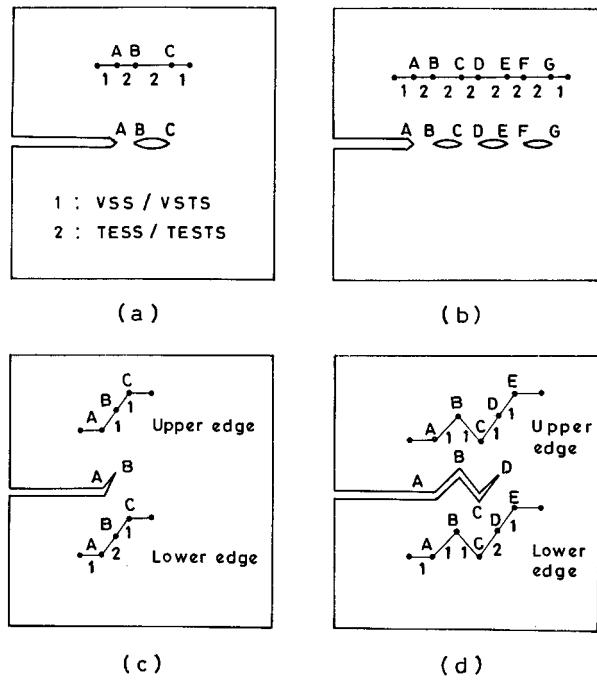


Figure 2. Modelling of neighbouring singularities. (a) Two neighbouring cracks. (b) Main crack and an array of microcracks. (c) Kinked crack. (d) Zigzag crack.

(1 in Figure 2(a)) can be considered at A and C. In the case of Figure 2(b) the elements can be used repeatedly to advantage to cover spans AB, BC, CD, DE, EF and FG. An ordinary singularity element can be employed at A and G. In the case of kinked crack (Figure 2(c)) the upper edge can be easily modelled by one end singularity elements. The bottom edge can be done through 1 two end singularity elements and 2 one end singularity elements. The arrangement of elements for the case of zigzag crack (Figure 2(d)) is shown.

MCCI-BASED COMPUTATION OF SIFS

The accuracy of the SIFs can be improved if the calculations are done through the energy release rates. One of the important methods to evaluate the strain energy release rate is Irwin's crack closure integral (CCI). It is first adapted in the finite element method (FEM) by Rybicki and Kanninen [31]. They described the method considering a linear variation of the displacement field (i.e. constant strain field) around the crack tip. They termed the method as modified crack closure integral (MCCI) technique. Later it has been shown by many investigators (e.g. Ramamurthy *et al.* [32], Maiti [33], etc.) that crack line displacement and stresses can be locally smoothed using the computed nodal data. These smoothed field can then be employed to compute the crack closure work. Recently the effectiveness of this method is also demonstrated in BEM [24–27] for linear, quadratic and quarter point elements around the crack tip. Here the procedure is outlined when a combination of two end singularity element and variable singularity element is used to analyse.

TESS and VSS element combination

In this combination the VSS element is employed to model the crack edge and the TESS element is used to represent the ligament ahead of the crack tip. In the MCCI-based calculations the crack closure work is evaluated taking note of the crack opening behind, and traction ahead of, the crack tip as per the initially assumed variations [25–27]. For this combination the crack opening displacement has a variation as per the VSS element (Equation (1)). The traction variation ahead of the crack tip is given by Equation (5).

$$v = b_1(1 - x/l)^c + b_2(1 - x/l)^{c+1} + b_3(1 - x/l) + b_4 \quad (11)$$

$$t = a_1(x/l)^c + a_2(x/l)^{c+1} + a_3(1 - x/l)^d + a_4(1 - x/l)^{d+1} + a_5(x/l) + a_6 \quad (12)$$

where $b_1 = (-2^c v_{j-2} + 2^{c+1} v_{j-1} - 2^c v_j)$, $b_2 = (2^c v_{j-2} - 2^{c+1} v_{j-1} + 2^c v_j)$, $b_3 = (v_{j-2} - v_j)$ and $b_4 = v_j$ and $a_1 = (-2^{c-1} t_{j+2} + 2^c t_{j+1} - 2^{c-1} t_j)$, $a_2 = (2^{c-1} t_{j+2} - 2^c t_{j+1} + 2^{c-1} t_j)$, $a_3 = (-2^{d-1} t_{j+2} + 2^d t_{j+1} - 2^{d-1} t_j)$, $a_4 = (2^{d-1} t_{j+2} - 2^d t_{j+1} + 2^{d-1} t_j)$, $a_5 = (t_{j+2} - t_j)$ and $a_6 = t_j$. v_j and t_j are the displacement and traction in the direction normal to the crack.

Remote mechanical loading. For this type of loading the mode I crack closure work is obtained [25] through

$$W_I = \frac{1}{2} \int_0^l vt \, dx \quad (13)$$

where l is the crack tip element size. For a symmetric crack configuration $v_j = 0$. For other cases displacements relative to the crack tip is to be considered. Combining (11) and (12)

$$\begin{aligned}
 W_1 = \frac{l}{2} \int_0^1 \{ & (1-z)^c z^c a_1 b_1 + (1-z)^{c+1} z^c a_1 b_2 + (1-z) z^c a_1 b_3 \\
 & + (1-z)^c z^{c+1} a_2 b_1 + (1-z)^{c+1} z^{c+1} a_2 b_2 + (1-z) z^{c+1} a_2 b_3 \\
 & + (1-z)^c (1-z)^d a_3 b_1 + (1-z)^{c+1} (1-z)^d a_3 b_2 + (1-z) (1-z)^d a_3 b_3 \\
 & + (1-z)^c (1-z)^{d+1} a_4 b_1 + (1-z)^{c+1} (1-z)^{d+1} a_4 b_2 + (1-z) (1-z)^{d+1} a_4 b_3 \\
 & + (1-z)^c z a_5 b_1 + (1-z)^{c+1} z a_5 b_2 + (1-z) z a_5 b_3 \\
 & + (1-z)^c a_6 b_1 + (1-z)^{c+1} a_6 b_2 + (1-z) a_6 b_3 \} dz
 \end{aligned} \tag{14}$$

where $z = x/l$. Finally the mode I strain energy release rate $G_I = W_1/l$ is obtained

$$\begin{aligned}
 G_I = [& v_{j-2}(c_1 a_1 + c_2 a_2 + c_3 a_3 + c_4 a_4 + c_5 a_5 + c_6 a_6) \\
 & + v_{j-1}(c_7 a_1 + c_8 a_2 + c_9 a_3 + c_{10} a_4 + c_{11} a_5 + c_{12} a_6)]/2
 \end{aligned} \tag{15}$$

where

$$\begin{aligned}
 c_1 &= [-2^c B(1+c, 1+c) + 2^c B(2+c, 1+c) + B(2, 1+c)] \\
 c_2 &= [-2^c B(1+c, 2+c) + 2^c B(2+c, 2+c) + B(2, 2+c)] \\
 c_3 &= [-2^c/(1+c+d) + 2^c/(2+c+d) + 1/(2+d)] \\
 c_4 &= [-2^c/(2+c+d) + 2^c/(3+c+d) + 1/(3+d)] \\
 c_5 &= [-2^c B(1+c, 2) + 2^c B(2+c, 2) + B(2, 2)] \\
 c_6 &= [-2^c/(1+c) + 2^c/(2+c) + 0.5] \\
 c_7 &= [2^{c+1} B(1+c, 1+c) - 2^{c+1} B(2+c, 1+c)] \\
 c_8 &= [2^{c+1} B(1+c, 2+c) - 2^{c+1} B(2+c, 2+c)] \\
 c_9 &= [2^{c+1}/(1+c+d) - 2^{c+1}/(2+c+d)] \\
 c_{10} &= [2^{c+1}/(2+c+d) - 2^{c+1}/(3+c+d)] \\
 c_{11} &= [2^{c+1} B(1+c, 2) - 2^{c+1} B(2+c, 2)] \\
 c_{12} &= [2^{c+1}/(1+c) - 2^{c+1}/(2+c)], \quad \text{and}
 \end{aligned} \tag{16}$$

$$B(m, n) = \int_0^1 (1-z)^{m-1} z^{n-1} dz \tag{17}$$

A similar expression can also be derived for a mode II crack. That is

$$G_{II} = [u_{j-2}(c_1 a_1 + c_2 a_2 + c_3 a_3 + c_4 a_4 + c_5 a_5 + c_6 a_6) + u_{j-1}(c_7 a_1 + c_8 a_2 + c_9 a_3 + c_{10} a_4 + c_{11} a_5 + c_{12} a_6)]/2 \quad (18)$$

where u is the crack sliding displacement. In defining a_i 's traction s_j , s_{j+1} and s_{j+2} must be used in place of t_j , t_{j+1} and t_{j+2} , respectively.

Crack edge pressure loading

For fluid pressure acting on the crack edges, the crack closure work is different

$$W_I = \frac{1}{2} \int_0^l vt \, dx + \frac{1}{2} \int_0^l vp \, dx \quad (19)$$

where p is fluid pressure acting to open a crack. Final expression for modes I and II energy release rates are obtained in the form

$$G_I = [v_{j-2}(c_1 a_1 + c_2 a_2 + c_3 a_3 + c_4 a_4 + c_5 a_5 + c_6 a_6 + c_6 p) + v_{j-1}(c_7 a_1 + c_8 a_2 + c_9 a_3 + c_{10} a_4 + c_{11} a_5 + c_{12} a_6 + c_{12} p)]/2 \quad (20)$$

$$G_{II} = [u_{j-2}(c_1 a_1 + c_2 a_2 + c_3 a_3 + c_4 a_4 + c_5 a_5 + c_6 a_6 + c_6 q) + u_{j-1}(c_7 a_1 + c_8 a_2 + c_9 a_3 + c_{10} a_4 + c_{11} a_5 + c_{12} a_6 + c_{12} q)]/2 \quad (21)$$

The constants a_i 's and c_i 's are already defined.

Thermal loading. To analyse a thermal stress problem, the usual heat transfer analysis must precede the stress analysis and relations (15) and (18) can be employed for the evaluations of modes I and II strain energy release rates. Similarly in the presence of thermal and a fluid pressure on the crack edges, relations (20) and (21) are to be employed. The thermal loading therefore can be treated as any mechanical loading.

TESTS and VSTS element combination

In this combination crack opening displacement is approximated by VSTS element and traction in ligament ahead of crack tip is by TESTS element. In this combination the traction is given by

$$t = a_1(x/l)^{c-1} + a_2(x/l)^c + a_3(1-x/l)^{d-1} + a_4(1-x/l)^d + a_5(x/l) + a_6 \quad (22)$$

where $a_1 = (-2^c t_{j+2} + 2^{c-1} t_{j+1} + 2^{c-1} t_j)$, $a_2 = (2^c t_{j+2} - 2^{c-1} t_{j+1} - 2^{c-1} t_j)$, $a_3 = (2^{d-1} t_{j+2} + 2^{d-1} t_{j+1} - 2^d t_j)$, $a_4 = (-2^{d-1} t_{j+2} - 2^{d-1} t_{j+1} + 2^d t_j)$, $a_5 = (t_{j+2} - t_j)$ and $a_6 = t_j$. The opening displacement field can be represented by Equation (11).

Following the procedure given for the energy calculation of the TESS element, modes I and II strain energy release rates for remote mechanical loading for this can be obtained. Explicitly

$$G_I = [v_{j-2}(c_1 a_1 + c_2 a_2 + c_3 a_3 + c_4 a_4 + c_5 a_5 + c_6 a_6) + v_{j-1}(c_7 a_1 + c_8 a_2 + c_9 a_3 + c_{10} a_4 + c_{11} a_5 + c_{12} a_6)]/2 \quad (23)$$

$$G_{II} = [u_{j-2}(c_1 a_1 + c_2 a_2 + c_3 a_3 + c_4 a_4 + c_5 a_5 + c_6 a_6) + u_{j-1}(c_7 a_1 + c_8 a_2 + c_9 a_3 + c_{10} a_4 + c_{11} a_5 + c_{12} a_6)]/2 \quad (24)$$

where

$$\begin{aligned} c_1 &= [-2^c B(1+c, c) + 2^c B(2+c, c) + B(2, c)] \\ c_2 &= [-2^c B(1+c, 1+c) + 2^c B(2+c, 1+c) + B(2, 1+c)] \\ c_3 &= [-2^c/(c+d) + 2^c/(1+c+d) + 1/(1+d)] \\ c_4 &= [-2^c/(1+c+d) + 2^c/(2+c+d) + 1/(2+d)] \\ c_5 &= [-2^c B(1+c, 2) + 2^c B(2+c, 2) + B(2, 2)] \\ c_6 &= [-2^c/(1+c) + 2^c/(2+c) + 0.5] \\ c_7 &= [2^{c+1} B(1+c, c) - 2^{c+1} B(2+c, c)] \\ c_8 &= [2^{c+1} B(1+c, 1+c) - 2^{c+1} B(2+c, 1+c)] \\ c_9 &= [2^{c+1}/(c+d) - 2^{c+1}/(1+c+d)] \\ c_{10} &= [2^{c+1}/(1+c+d) - 2^{c+1}/(2+c+d)] \\ c_{11} &= [2^{c+1} B(1+c, 2) - 2^{c+1} B(2+c, 2)] \\ c_{12} &= [2^{c+1}/(1+c) - 2^{c+1}/(2+c)] \end{aligned} \quad (25)$$

For a crack edge pressure loading and/or remote mechanical loading G_I and G_{II} are as follows:

$$G_I = [v_{j-2}(c_1 a_1 + c_2 a_2 + c_3 a_3 + c_4 a_4 + c_5 a_5 + c_6 a_6 + c_6 p) + v_{j-1}(c_7 a_1 + c_8 a_2 + c_9 a_3 + c_{10} a_4 + c_{11} a_5 + c_{12} a_6 + c_{12} p)]/2 \quad (26)$$

$$G_{II} = [u_{j-2}(c_1 a_1 + c_2 a_2 + c_3 a_3 + c_4 a_4 + c_5 a_5 + c_6 a_6 + c_6 q) + u_{j-1}(c_7 a_1 + c_8 a_2 + c_9 a_3 + c_{10} a_4 + c_{11} a_5 + c_{12} a_6 + c_{12} q)]/2 \quad (27)$$

where the coefficients a_i and c_i are given by Equations (22) and (25), respectively. In the presence of thermal and/or mechanical loading modes I and II strain energy release rates can be evaluated using the above equations appropriately.

Evaluation of SIFs. The coefficients c_n are evaluated using

$$B(m, n) = \Gamma(m) \Gamma(n) / \Gamma(m + n) \quad (28)$$

$$\Gamma(n) = \lim_{j \rightarrow \infty} \frac{j! j^n}{n(n+1)(n+2)\dots(n+j)} \quad n \neq 0, -1, -2, \dots \quad (29)$$

For a particular c , the gamma function is calculated using double-precision arithmetic and $j = 50\,000$. It must be emphasised that the SIFs can be evaluated from G_I and G_{II} as their correlation are known only for $c = 0.5$. In other cases the MCCI-based relations can be employed just to calculate the strain energy release rates.

CASE STUDIES

Five case studies, involving a macrocrack and neighbouring microcracks subjected to mode I and mixed-mode mechanical loading, are presented. The computation is performed on a PC486 using single-precision arithmetic. For all the case studies a plane state of stress has been assumed. Both partial and total modelling of singularities have been considered. Partial modelling has been obtained employing the combination of TESS and VSS elements. TESTS and VSTS elements are used for total modelling of singularities.

Edge crack with collinear neighbouring microcrack. This example deals with an edge crack with a collinear neighbouring microcrack in a flat plate under uniformly distributed load (Figure 3(a)). The major dimensions are: plate width $W = 20$ mm, $L/W = 3$ and $a/W = 0.5$. The distance between the edge crack tip and the microcrack tip $AB = \delta = 0.05a$. The selected material properties are: elastic modulus $E = 1$ MPa and Poisson's ratio $\nu = 0.3$. The uniformly distributed load $\sigma = 10$ MPa. The length of the microcrack BC ($2l$) is varied to obtain $\delta/2l$ in the range 0.125 to 1 keeping δ constant. Half of the plate is modelled (Figure 3(b)). AB is modelled with a two end singularity element with $c = 0.5$ and $d = 0.5$. The element on the crack edge and terminating at A is a variable singularity element. The microcrack $2l$ is simulated by a two end singularity element with $c = 0.5$ and $d = 0.5$ when $\delta/2l = 1$. For other values of $\delta/2l$ it is covered by either two variable singularity elements, or two variable singularity elements and one or more quadratic elements. The element near C on the ligament side is another variable singularity element. Total number of elements vary from 21 ($\delta/2l = 1$) to 24 ($\delta/2l = 0.125$). The size of crack tip elements near A is 5 per cent a . The SIF at the main crack tip A has been evaluated employing the proposed MCCI-based correlations (Equations (15) and (23)). This example has earlier been studied by Chudnovsky and Kachanov [1], Kachanov [2] and Maiti [12]. The computed SIFs are compared with Kachanov [2] and Maiti [12] in Figure 3(c) and Table I. In Figure 3(c) the SIF correction factor $Y (Y = K_I/K_{I0})$ is plotted. Here K_{I0} is $158.6 \text{ N mm}^{-3/2}$. The presence of the microcrack causes an enhancement of the SIF at A for lower value of $\delta/2l$. As $\delta/2l$ is increased ($\delta/2l = 1$) the effect is insignificant and the computed value reduces to the corresponding value in the absence of the microcrack. The SIF is also computed using the displacement method at the first and second element end nodes. These results are inferior to those based on the MCCI calculations.

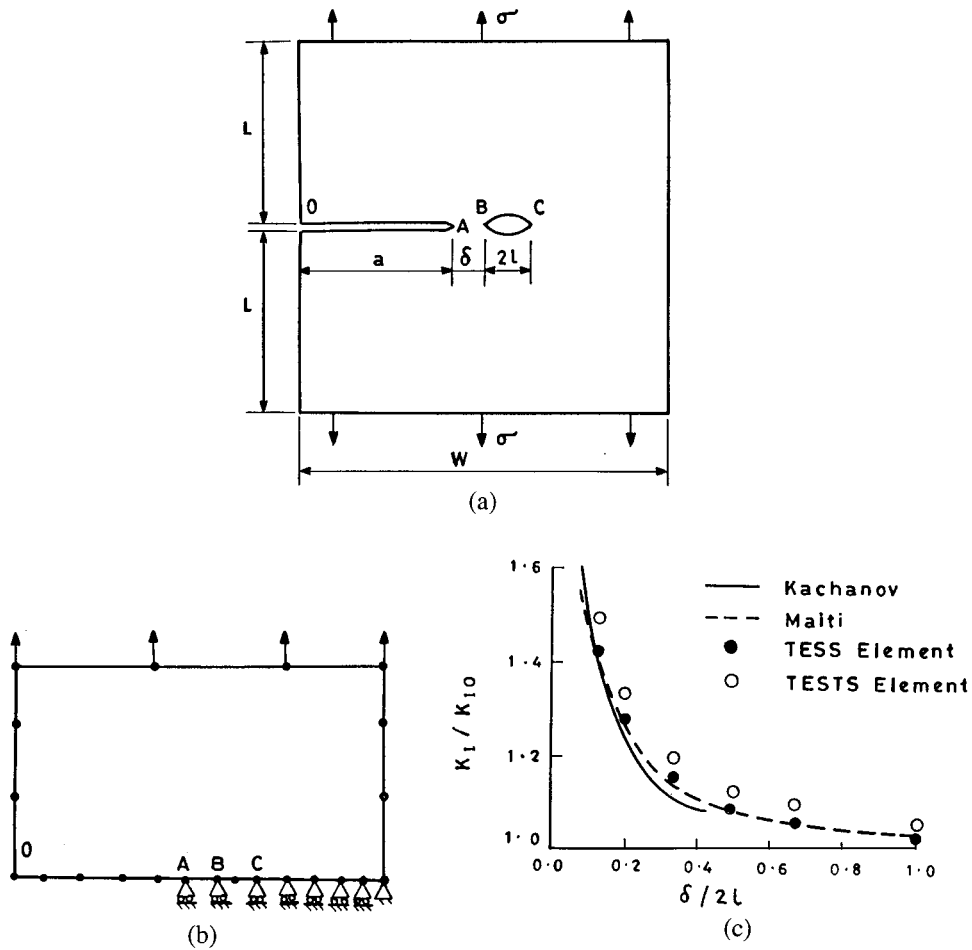


Figure 3. (a) Edge crack with collinear neighbouring crack. (b) Boundary element mesh. (c) Comparison of SIFs.

Table I. Comparison of SIFs for collinear neighbouring cracks.

$\delta/2l$	SIF ($N\text{ mm}^{-3/2}$)		
	Maiti [12]	TESS element	TESTS element
0.125	225.520	225.678	236.259
0.200	200.920	202.358	210.848
0.333	181.860	183.222	189.905
0.500	171.900	173.025	178.632
0.667	162.630	168.277	173.024
1.000	162.630	162.984	167.280

The effect of variation of the order of integration on the SIFs have been shown in Table II. The order is varied from 4 to 16. The associated Gauss point co-ordinates and weights are obtained from Stroud and Secrest [30]. For the TESS element, the SIF almost stabilizes around 8. For the TESTS element a higher order of integration is preferable.

The effect of modelling the two neighbouring crack tips by two end variable singularity element and alternatively by one end singularity elements is examined. The two crack tips A and B can be simulated by two one end variable singularity elements and the intermediate span can be covered by one or more of quadratic elements. These arrangements are indicated by 2VSS + 1QE or 2VSTS + 1QE in Table III. It may also be simulated by two variable singularity elements. These arrangements are indicated by 2VSS or 2VSTS. Obviously, the most attractive choice is to use merely a two end singularity element. These schemes are indicated by 1TESS or 1TESTS. The effect of such modelling on the computed SIFs are presented in Table III. Both partial and total modelling have been considered. The first three columns indicate the partial case. The other three represents to full modelling. The crack tip element size in the first case is $0.05a/3$, in second case $0.025a$ and it is $0.05a$ in the last case when TESS/TESTS elements are employed. The computed results for all the three sets are comparable. The advantage offered by the new elements is therefore quite evident.

Edge crack with neighbouring stacked parallel cracks. The presence of a microcrack can cause an 'amplification' of the SIF as illustrated in the previous example or 'shielding' depending on its location. This example deals with the latter (Figure 4(a)). The plate dimensions are $W = 20$ mm, $L/W = 5$ and $a/W = 0.5$. The size of the microcrack $2l = 0.05a$. The location of the microcrack is

Table II. Effect of variation of Gauss quadrature on SIFs for collinear neighbouring cracks.

$\delta/2l$	SIF ($\text{N mm}^{-3/2}$)				
	Order of Gauss quadrature				
	4	8	10	12	16
TESS element					
0.125	226.433	225.715	225.679	225.672	225.678
0.200	202.994	202.402	202.363	202.355	202.358
0.333	183.786	183.271	183.231	183.224	183.222
0.500	173.557	173.076	173.040	173.029	173.025
0.667	168.815	168.340	168.300	168.286	168.277
1.000	163.465	163.036	163.002	162.991	162.984
TESTS element					
0.125	253.775	240.646	238.686	237.525	236.259
0.200	226.729	214.954	213.139	212.055	210.848
0.333	204.480	193.790	192.094	191.068	189.905
0.500	192.533	182.418	180.783	179.781	178.632
0.667	186.658	176.818	175.193	174.187	173.024
1.000	180.446	170.978	169.402	168.421	167.280

Table III. Effect of modelling of two collinear neighbouring crack tips on SIFs.

$\delta/2l$	SIF ($N\text{ mm}^{-3/2}$)					
	No. of elements employed to model two collinear neighbouring crack tips					
	2VSS + 1 ^a	2VSS	1TESS	2VSTS + 1 ^a	2VSTS	1TESTS
0.125	223.514	222.732	225.678	228.657	229.115	236.259
0.200	200.168	199.644	202.358	204.580	204.973	210.848
0.333	181.284	180.939	183.222	185.034	185.341	189.905
0.500	171.458	171.187	173.025	174.810	175.040	178.632
0.667	167.017	166.768	168.277	169.894	170.070	173.024
1.000	162.266	162.040	162.984	165.111	165.218	167.278

^a implies one quadratic element has been used in between two VSS/VSTS elements

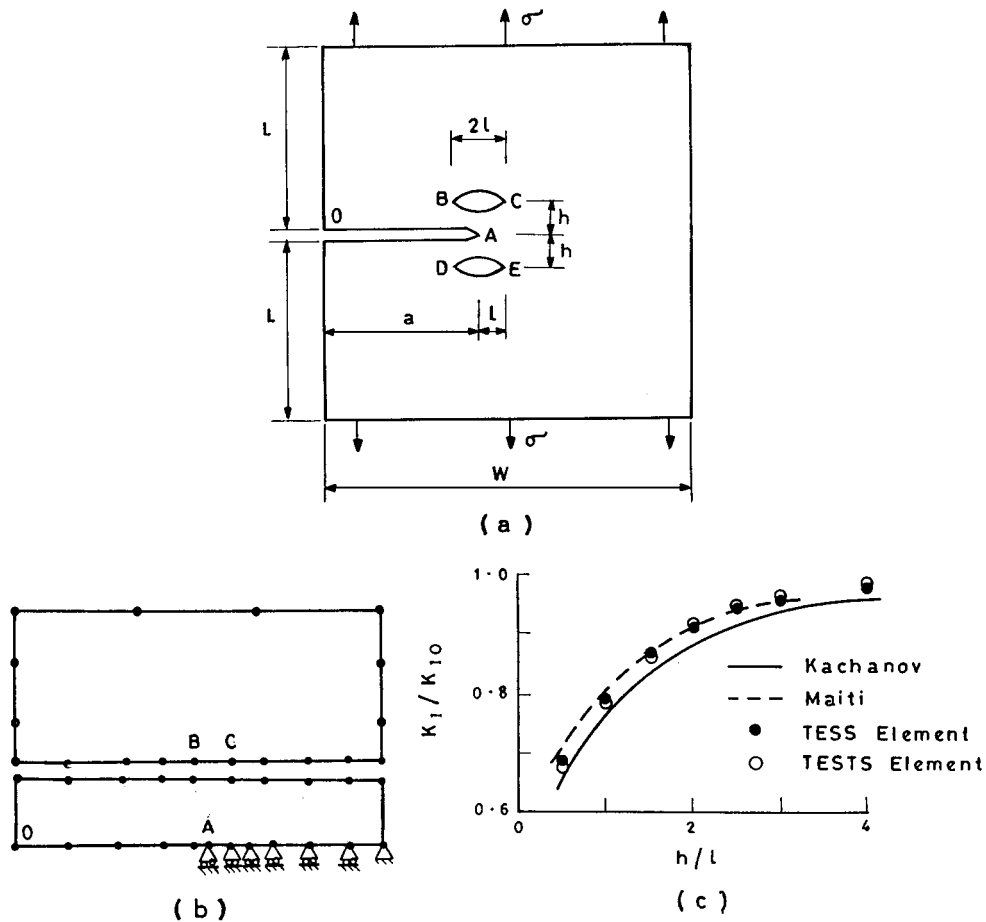


Figure 4. (a) Edge crack with neighbouring stacked parallel cracks. (b) Boundary element mesh. (c) Comparison of SIFs.

assumed to cause a maximum shielding effect [2]. The influence of vertical distance h on the shielding effect is examined. h/l is varied from 0.5 to 4 keeping l constant. The material properties are the same as in the previous example. The plate is subjected to a uniform tension $\sigma = 10$ MPa.

Half of the plate is modelled. The subregion analysis is adapted (Figure 4(b)). The main crack tip is modelled with a variable singularity element. The whole span of the microcrack $2l$ is covered by a two end singularity element and the adjoining elements at the two crack tips are the variable singularity elements. The total number of elements employed are 42. The size of the elements near the crack tip A is 2.5 per cent a . The SIF is determined at the main crack tip A based on the MCCI method. The problem has earlier been studied by Kachanov [2] and Maiti [12]. The results are compared in Figure 4(c) and Table IV. In Figure 4(c) the variation of SIF correction factor Y ($Y = K_I/K_{I0}$, where $K_{I0} = 158.6 \text{ N mm}^{-3/2}$) is plotted. The shielding effect is pronounced as the cracks are in close proximity, e.g. lower value of h/l . The effect reduces as h/l is increased. For $h/l > 3$ the SIF is almost equal to the SIF at the tip A of the maincrack in the absence of the microcracks. In this case too the SIF is calculated based on the displacement method at the first and second end nodes. These differ considerably with the reference solutions. Particularly for low value of h/l ($h/l = 0.5$ and $h/l = 1$), the computed SIF by the displacement method is more than the reference solution by 50 per cent or so; as a result the shielding effect does not properly emerge. Because of this poor accuracy they have not been included.

The effect of variation of order of integration on the computed SIFs are examined (Table V). The order is varied from 4 to 16. Similar trend as in the previous example is observed.

Edge crack surrounded by three neighbouring microcracks. This example deals with an edge crack surrounded by three neighbouring microcracks in a plate under mode I uniformly distributed loading (Figure 5). Out of the three microcracks BC is collinear. The other two DE and FG are symmetrically located with respect to the main crack. The major dimensions are: $W = 20$ mm, $L/W = 3$ and $a/W = 0.5$. The horizontal distance from the main crack tip A to the three microcrack tips B, D and F are δ and $\delta/a = 0.02$. The span of microcrack $2l = 0.05a$ (i.e. $\delta/2l = 0.4$). The vertical distance of D and F from the crack edge is h and $h/l = 1$. The crack angle θ is varied from 0 to 180°. The material properties are: $E = 210$ GPa, $\nu = 0.3$. The load intensity $\sigma = 10$ MPa. Half of the plate is modelled due to the symmetry. The subregion analysis is adapted. One region includes the main crack OA, the microcracks BC and ED. In fact, ED is also present in the other region which includes the remaining part of the upper half plate. The

Table IV. Comparison of SIFs for stacked parallel cracks.

$\delta/2l$	SIF ($\text{N mm}^{-3/2}$)		
	Maiti [12]	TESS element	TESTS element
0.5	113.480	108.762	106.786
1.0	125.830	120.798	118.248
1.5		137.445	136.350
2.0	144.250	145.170	145.095
2.5		149.391	149.964
3.0	150.100	151.958	152.956
4.0		154.805	156.288

Table V. Effect of variation of Gauss quadrature on SIFs for stacked parallel cracks.

$\delta/2l$	SIF ($\text{N mm}^{-3/2}$)					
	Maiti [12]	Order of Gauss quadrature				
		4	8	10	12	16
TESS element						
0.5	113.480	111.613	110.075	109.639	109.276	108.762
1.0	125.830	122.734	121.168	121.274	121.118	120.798
1.5		138.694	137.573	137.690	137.607	137.445
2.0	144.250	146.223	145.255	145.304	145.247	145.170
2.5		150.382	149.475	149.478	149.436	149.391
3.0	150.100	152.924	152.054	152.026	151.994	151.958
4.0		155.718	154.900	154.857	154.830	154.805
TESTS element						
0.5	113.480	119.837	108.625	107.895	107.248	106.786
1.0	125.830	135.417	123.661	121.771	120.267	118.248
1.5		151.451	140.916	139.252	137.985	136.350
2.0	144.250	159.571	149.384	147.726	146.551	145.095
2.5		164.208	154.143	152.473	151.342	149.964
3.0	150.100	167.104	157.087	155.404	154.298	152.956
4.0		170.347	160.367	158.683	157.596	156.288

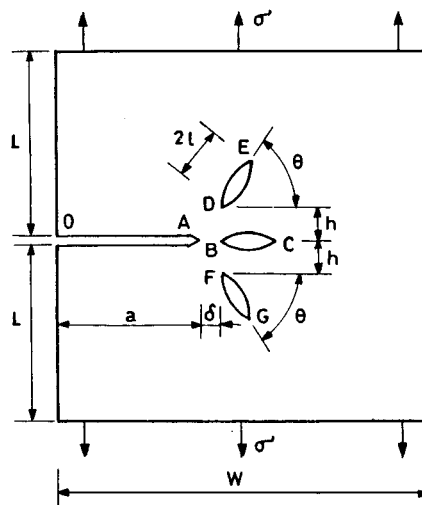


Figure 5. Edge crack with three collinear cracks.

discretization employed is similar to the previous example. The span AB is covered by a two end singularity element. The microcracks BC and DE are modelled using the similar elements. The variable singularity elements are employed on the crack edge behind the main crack tip A, and in front of the microcrack tips C and E. The size of crack tip elements at A is 2 per cent a .

This problem is studied employing an order of integration 16. The SIF correction factor Y ($Y = K_I/K_{I0}$) is evaluated at A employing MCCI-based calculations (Figure 6). The SIF at A due to the presence of only the collinear microcrack BC is also evaluated. This is 1.126 for the TESS element and 1.16 for the TESTS element. The computed Y considering all the three microcracks show that DE and FG have an amplification effect for $\theta = 0-75^\circ$. The computed Y is maximum at $\theta = 15^\circ$, though the variation is not significant up to a value of $\theta = 30^\circ$. As $\theta \geq 90^\circ$, the shielding effect begins. For $\theta \geq 150^\circ$, the K_I is less than K_{I0} . At $\theta = 180^\circ$, the K_I is $0.8 K_{I0}$ (i.e. $Y \approx 0.8$). All computed values of Y are given in Table VI.

The effect of the vertical distance h on the SIF at the tip A is also examined. The problem is analysed for $h/l = 2$ by varying h and keeping all other parameters the same. The computed Y are presented in Figure 6 and Table VI. The influence of the microcracks DE and FG, as expected, are less pronounced. The SIF correction factor Y is again maximum at $\theta \approx 15^\circ$ and the change in Y is less up to $\theta = 30^\circ$. For this arrangement the shielding effect is observed for $\theta \approx 105^\circ$ and more. However, the shielding effect is less in the previous arrangement. Further, for $\theta = 180^\circ$ the Y is more than 1; i.e. there is amplification of the SIF.

Zigzag crack with microcrack. A zigzag crack may appear due to stress corrosion cracking. Here a zigzag crack is considered with three kinks (Figure 7). At every knee point there is a singularity,

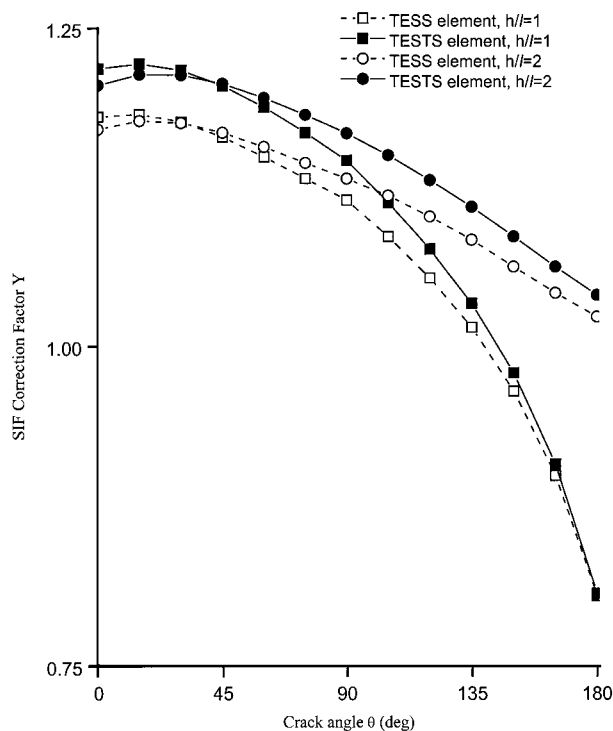


Figure 6. Variation of SIF correction factor Y with crack angle for edge crack with three adjacent microcracks (Figure 5).

Table VI. Variation of SIF correction factor Y for edge crack with three adjacent microcracks (Figure 5) with microcrack angle.

θ (deg.)	SIF correction factor Y ($Y = \text{SIF}/Y_0$)			
	$h/l = 1$		$h/l = 2$	
	TESS	TESTS	TESS	TESTS
0.0	1.1801	1.2181	1.1702	1.2051
15.0	1.1821	1.2219	1.1770	1.2136
30.0	1.1763	1.2170	1.1754	1.2133
45.0	1.1644	1.2050	1.1678	1.2065
60.0	1.1489	1.1881	1.1567	1.1954
75.0	1.1320	1.1680	1.1442	1.1819
90.0	1.1150	1.1461	1.1318	1.1674
105.0	1.0863	1.1132	1.1185	1.1503
120.0	1.0540	1.0766	1.1021	1.1307
135.0	1.0151	1.0339	1.0838	1.1097
150.0	0.9651	0.9794	1.0630	1.0864
165.0	0.8994	0.9081	1.0422	1.0629
180.0	0.8051	0.8068	1.0235	1.0406

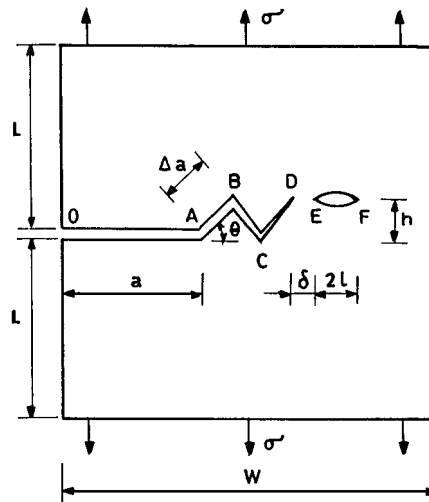


Figure 7. A zigzag crack with a neighbouring crack.

whose order depends on the included angle [7]. When the lengths of the kinks (AB, BC and CD) are small the singularities will interact. The presence of a microcrack ahead will enhance the SIF at the crack tip D. The main crack is an edge crack in a plate under uniformly distributed load. The major problem dimensions are $L/W = 3$, $a/W = 0.5$, $W = 20$ mm, $\theta = 45^\circ$ and $\theta = 5$ per cent a . The length of the kinks (Δa) AB, BC and CD are identical and $\Delta a = 2$ per cent a .

The included angles at all the knees is 90° . The length $2l$ of the microcrack EF is varied keeping DE ($= \delta$) constant to obtain $\delta/2l$ in the range of 0.125–1.0. The vertical distance $h/\Delta a = \sin 45^\circ$. The material properties are the same as in the previous example. The uniform tension $\sigma = 10$ MPa. The full plate is modelled. Again subregion analysis is adapted. Each region consists of 27 elements. The spans AB, BC and CD are covered by two end singularity elements. The elements behind the crack tips A and E, and ahead of the crack tips D and F are variable singularity elements. EF is a two end singularity element for $\delta/2l = 0.5$ and 1. Otherwise EF is modelled with variable singularity element.

This problem is studied employing an order of integration 16. The results on the SIF correction factor Y ($Y = K_I/K_{I0}$, where $K_{I0} = 158.6 \text{ N mm}^{-3/2}$) at the tip D are presented (Figure 8(a)). No data are available in the literature for a comparison. The presence of the crack EF leads to an enhancement of the SIF at D for low values of $\delta/2l$. As $\delta/2l$ increases the effect reduces. For $\delta/2l = 1$ the SIF reduces to the corresponding value of the SIF without the presence of EF. Both the modes I and II SIFs are significant, though the mode I SIF is dominant.

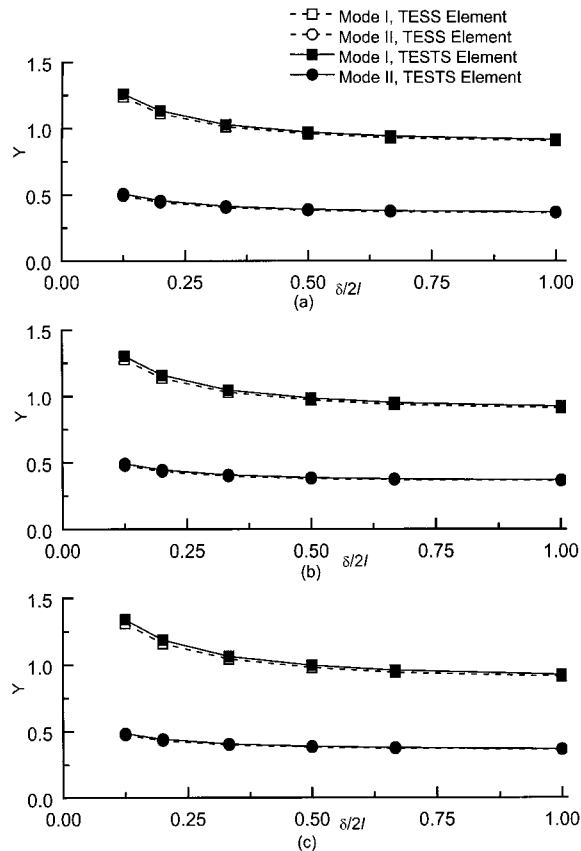


Figure 8. Effect of intercrack distance, microcrack size and vertical distance of microcrack on Y for a zigzag crack and a microcrack. Vertical distance for (a) h (b) $h/2$ and (c) 0 .

The influence of vertical distance h is studied. Two cases; $h/\Delta a = \sin 45^\circ/2$ and 0 are considered. A very similar discretization with a little readjustment of elements is employed. The variation of the SIF correction factor Y (Figure 8(b) and (c)) shows a similar trend. h does not seem to have much effect on Y though it increases slightly when EF is located closer to the main crack tip A. For example, for $\delta/2l = 0.125$, the increase in Y as $h/\Delta a$ is varied from $\sin 45^\circ$ to 0 is 8 per cent.

Kinked crack emanating from circular hole. The problem geometry is shown (Figure 9). This type of a problem has earlier been solved by Isida *et al.* [34] adapting body force method and Mogilevskaya [35] employing complex hypersingular integral equation. The kink AB is at an angle 45° and the angle (θ) between AB and BC is 90° (Figure 9). The singularities exist at A and B. The radius of the circular hole R is varied to obtain a/R in the range 0.1–1.0 keeping a constant. The material properties are similar to that considered in the previous example. The subregion analysis is adapted (Figure 9(b)). The span AB is covered by a two end variable singularity element. The elements behind the kink tip A and ahead of the crack tip B are variable singularity elements. The boundary of the circular hole is approximated by 12 quadratic elements for $a/R = 0.1$ and 0.2; and eight elements for $a/R = 0.5$ and 1. The adapted mesh to model the circular hole is relatively coarse here. As an example Mogilevskaya [35] has employed 80 elements for $a/R = 0.1$ and 40 for $a/R = 0.2$. Two cases of loading, uniaxial ($\sigma_x = 0, \sigma_y = 10$) and biaxial ($\sigma_x = \sigma_y = 10$) are considered.

The SIF correction factor Y ($Y = K_I/\sigma\sqrt{(\pi a)}$ or $K_{II}/\sigma\sqrt{(\pi a)}$) are evaluated based on the proposed MCCI method and presented in Table VII. The computed results are in good agreement with the results of both Isida *et al.* [34] and Mogilevskaya [35] (Table VII). The maximum difference from the results of Isida *et al.* is less than 2 per cent.

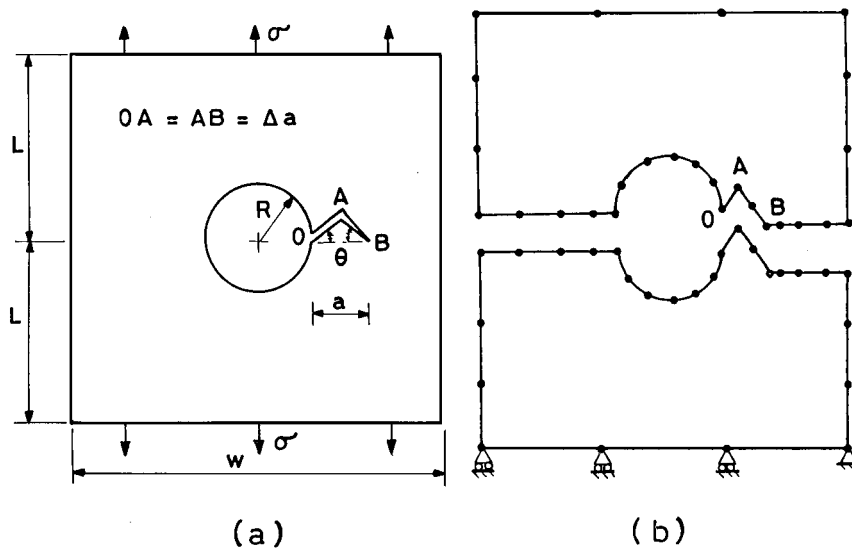


Figure 9. (a) Kinked crack emanating from a circular hole. (b) Boundary element mesh.

Table VII. SIF correction factor for a kinked crack emanating from a circular hole in a plane.

a/R	SIF correction factor Y							
	Isida <i>et al.</i> [34]		Mogilevskaya [35]		TESS		TESTS	
	Y_I	Y_{II}	Y_I	Y_{II}	Y_I	Y_{II}	Y_I	Y_{II}
Uniaxial tension								
0.1	2.0920	-1.0340	2.0940	-1.0465	2.1173	-1.0532	2.1341	-1.0545
0.2	1.8030	-0.8660	1.8065	-0.8757	1.8277	-0.8744	1.8389	-0.8733
0.5	1.3140	-0.6240	1.3175	-0.6319	1.3085	-0.6192	1.3218	-0.6179
1.0	0.9700	-0.5060	0.9736	-0.5084	0.9502	-0.4964	0.9551	-0.4975
Biaxial tension								
0.1	1.4930	-0.7540	1.4937	-0.7628	1.5136	-0.7674	1.5210	-0.7691
0.2	1.3620	-0.6750	1.3647	-0.6818	1.3767	-0.6827	1.3898	-0.6819
0.5	1.1270	-0.5310	1.1321	-0.5402	1.1102	-0.5417	1.1252	-0.5404
1.0	0.9450	-0.4190	0.9636	-0.4184	0.9259	-0.4271	0.9361	-0.4256

DISCUSSION AND CONCLUSIONS

A pair of two end variable order singularity boundary elements are introduced. The first element, the two end strain singularity (TESS) element, partially models the singularity behaviour; it models only the variable order strain singularity at both the ends of the element. The second element, the two end strain and traction singularity (TESTS) element, can simulate the singularity in both the strain and traction at both the ends of the element. The shape functions adapted to impose the singularity in the variation of traction at both the ends are obtained from the derivative of the shape functions for the displacement. Relations are given to compute the strain energy release rate based on the modified crack closure integral (MCCI) technique for both these elements; SIFs can be evaluated for the case of square root singularity at the crack tip. From the case studies it is evident that the computed results are in good agreement with the other published results based on analytical method or FEM.

Since the terms of matrices $[H]$ and $[G]$ are obtained through Gauss quadrature the accuracy of displacements and tractions, and hence the SIFs, depend on the order of the numerical integration. For the case of TESS element the fundamental solution is multiplied by $(r/l)^c$ and $(1 - r/l)^d$. The order of singularity in the fundamental solution for displacement depends on $[\ln(1/r) \times (r)^c]$ and $[\ln(1/r) \times (l - r)^d]$. However, in the case of fundamental solution for the traction this depends on $[(1/r) \times (r)^c]$ and $[(1/r) \times (l - r)^d]$. In the case of TESTS element, the fundamental solution for traction is multiplied by $(r/l)^c$ and $(1 - r/l)^d$; thereby making the order of singularity to depend on $[(1/r) \times (r)^c]$ and $[(1/r) \times (l - r)^d]$. The fundamental solution of displacement is multiplied by $(r/l)^{c-1}$ and $(1 - r/l)^{d-1}$. The order of singularity here is guided by $[\ln(1/r) \times (1/r)^{1-c}]$ and $[\ln(1/r) \times (1/(l - r))^{d-1}]$. The order of singularity in the case of TESTS element is more powerful than in the case of the TESS element. The computed traction near the crack tip varies with the order of integration, though the displacements do not change much for the TESTS element. Hence the SIF when computed by displacement method stabilizes for

a moderate integration order. When calculations are performed through the MCCI technique, a higher-order integration, 10 or more, is required in the case of TESTS element compared to TESS element for the same degree of accuracy. In general, the TESTS element seems to have an edge over the TESS element notwithstanding the requirement of a higher integration order.

Finally, the conclusions are as follows:

- (i) The variable order singularity at two neighbouring points can be modelled using a single boundary element. The element shape functions are obtained through a simple manipulation of the shape functions of the parent 3-noded element shape functions. Two elements have been suggested.
- (ii) Partial modelling of strain singularity at both the ends of an element is possible through an element like the TESS element whereas a full simulation of strain and traction singularities simultaneously is possible employing the TESTS element.
- (iii) Both the elements satisfy the rigid-body mode and the constant-strain criteria.
- (iv) An integration order of 10 or so is preferable when adapting the TESTS element.
- (v) The proposed elements offer an attractive method of handling problems involving crack–crack interaction.
- (vi) The strain energy release rates G_I and G_{II} can be evaluated from the crack opening displacements and tractions near the crack tip using the MCCI relations irrespective of the order of singularity. The SIFs can be derived from G_I and G_{II} only in the case of square-root singularity.
- (vii) The presence of neighbouring singularities substantially influence the SIF at the tip of the main crack. There can be an amplifying or a shielding effect depending on the locations and sizes of the microcracks.

LIST OF SYMBOLS

a	crack length
a_n	coefficients of traction
$B(m, n)$	Beta function
b_n	coefficients of displacement
c, d	singularity parameter
c_n	coefficients used in MCCI calculation
E	elastic modulus
G_I, G_{II}	strain energy release rate in modes I and II
h	length
K_I, K_{II}	stress intensity factors
l	crack tip element size/length of microcrack
N_i, M_i	shape functions
p, q	components of crack edge loading normal and parallel to crack
r	distance from crack tip
s, t	components of traction parallel and normal to crack
u, v	components of displacement parallel and normal to crack
W	geometric dimensions of domain
W_I, W_{II}	crack closure work

x, y	Cartesian co-ordinates
Y	SIF correction factor
Δa	kink length
δ	distance from main crack tip to that of the neighbouring microcrack
θ	crack orientation with the x -axis
ν	Poisson's ratio
ξ	natural co-ordinate
ϕ	potential/temperature
$\Gamma(m)$	Gamma function

REFERENCES

1. Chudnovsky A, Kachanov M. Interaction of a crack with a field of microcracks. *International Journal of Engineering Science* 1983; **21**:1009–1018.
2. Kachanov M. On crack-microcrack interaction. *International Journal of Fracture* 1986; **30**:R65–R72.
3. Raju IS. Calculation of strain energy release rates with higher order and singular finite elements. *Engineering Fracture Mechanics* 1987; **28**:251–264.
4. Hori M, Nemat-Nasser S. Interacting micro-cracks near the tip in the process zone of a macro-crack. *Journal of the Mechanics and Physics of Solids* 1987; **35**:601–629.
5. Rubenstein AA, Choi HC. Macrocrack interaction with transverse array of microcracks. *International Journal of Fracture* 1988; **36**:15–26.
6. Lam KY, Phua SP. Multiple crack interaction and its effect on stress intensity factor. *Engineering Fracture Mechanics* 1991; **40**:585–592.
7. Williams ML. Stress singularities resulting from various boundary conditions in angular ends of plates in extension. *Journal of Applied Mechanics*, ASME, 1952; **19**:526–528.
8. Tracey DM, Cook TS. Analysis of power type singularities using finite elements. *International Journal for Numerical Methods in Engineering* 1977; **11**:1225–1233.
9. Stern M. Families of consistent conforming elements with singular fields. *International Journal for Numerical Methods in Engineering* 1979; **14**:409–421.
10. Maiti SK. A finite element for variable order singularities based on the displacement formulation. *International Journal for Numerical Methods in Engineering* 1992; **33**:1955–1974.
11. Dutta BK, Maiti SK, Kakodkar A. On the use of one point and two points singularity elements in the analysis of kinked cracks. *International Journal for Numerical Methods in Engineering* 1990; **29**:1487–1499.
12. Maiti SK. A multicorner variable order singularity triangle to model neighbouring singularities. *International Journal for Numerical Methods in Engineering* 1992; **35**:391–408.
13. Blandford GE, Ingraffea AR, Liggett JA. Two dimensional stress intensity factor computations using the boundary element method. *International Journal for Numerical Methods in Engineering* 1981; **17**:387–404.
14. Martinez J, Dominguez J. On the use of quarter-point boundary elements for stress intensity factor computations. *International Journal for Numerical Methods in Engineering* 1984; **20**:1941–1950.
15. Gangming L, Yongyuan Z. Improvement of stress singular element for crack problems in three dimensional boundary element method. *Engineering Fracture Mechanics* 1988; **31**:993–999.
16. Aliabadi MH, Rooke DP, Cartwright DJ. Fracture-mechanics weight-functions by the removal of singular fields using boundary element analysis. *International Journal of Fracture* 1989; **40**:271–284.
17. Zang WL, Gudmundson P. Contact problems of kinked cracks modelled by a boundary integral method. *International Journal for Numerical Methods in Engineering* 1990; **29**:847–860.
18. Watson JO. Singular boundary elements for the analysis of cracks in plane strain. *International Journal for Numerical Methods in Engineering* 1995; **38**:2389–2411.
19. Chandra A, Huang Y, Wei X, Hu KX. A hybrid micro-macro BEM formulation for micro-crack clusters in elastic components. *International Journal for Numerical Methods in Engineering* 1995; **38**:1215–1236.
20. Saez A, Gallego R, Dominguez J. Hypersingular quarter-point boundary elements for crack problems. *International Journal for Numerical Methods in Engineering* 1995; **38**:1681–1701.
21. Chen WH, Chen TC. An efficient dual boundary element technique for a two-dimensional fracture problem with multiple cracks. *International Journal for Numerical Methods in Engineering* 1995; **38**:1739–1756.
22. Mukhopadhyay NK, Maiti SK, Kakodkar A. Effect of modelling of traction and thermal singularities on accuracy of SIFs computation through modified crack closure integral in BEM. *Engineering Fracture Mechanics* 1999; **64**:141–159.
23. Mukhopadhyay NK, Maiti SK, Kakodkar A. Variable singularity boundary element and its applications in computation of SIFs. *Computers and Structures* 1999, in press.

24. Farris TN, Liu M. Boundary element crack closure calculation of three-dimensional stress intensity factors. *International Journal of Fracture* 1993; **60**:33–47.
25. Mukhopadhyay NK, Maiti SK, Kakodkar A. Further considerations in modified crack closure integral based computation of stress intensity factor in BEM. *Engineering Fracture Mechanics* 1998; **59**:269–279.
26. Mukhopadhyay NK, Maiti SK, Kakodkar A. BEM based evaluation of SIFs using modified crack closure integral technique under remote and/or crack edge loading. *Engineering Fracture Mechanics* 1998; **61**:655–671.
27. Mukhopadhyay NK, Maiti SK, Kakodkar A. Modified crack closure integral based computation of SIFs for 2-D thermoelastic problems through BEM. *Nuclear Engineering and Design* 1999; **187**:277–290.
28. Brebbia CA, Dominguez J. *Boundary Elements an Introductory Course*. McGraw-Hill: London, 1982.
29. Becker AA. *The Boundary Element Method in Engineering—A Complete Course*. McGraw-Hill: London, 1992.
30. Stroud AH, Secrest D. *Gaussian Quadrature Formulas*. Prentice-Hall: New York, 1966.
31. Rybicki EF, Kanninen MF. A finite element calculation of stress intensity factors by a modified crack closure integral. *Engineering Fracture Mechanics* 1977; **9**:931–938.
32. Ramamurthy TS, Krishnamurthy T, Badri Narayan K, Vijaykumar K, Duttaguru B. Modified crack closure integral methods with quarter point elements. *Mechanics of Research and Communications* 1986; **13**:179–186.
33. Maiti SK. Finite element computation of crack closure integrals and stress intensity factors. *Engineering Fracture Mechanics* 1992; **41**:339–348.
34. Isida M, Cheng D, Nisitani H. Plane problems of an arbitrary array of cracks emanating from the edge of an elliptical hole. *Transaction of the Japanese Society of Mechanical Engineers* 1984; **50**(451):330–340.
35. Mogilevskaya SG. Numerical modelling of 2-D smooth crack growth. *International Journal Fracture* 1997; **87**:389–405.